Characterizing the phases of Langmuir monolayers of cylindrical brushes with x-ray reflectivity and diffraction

2005 J. Phys.: Condens. Matter 17 S685

(http://iopscience.iop.org/0953-8984/17/9/024)

INSTITUTE OF PHYSICS PUBLISHING JOURNAL OF PHYSICS: CONDENSED MATTER

J. Phys.: Condens. Matter **17** (2005) S685–S701 doi:10.1088/0953-8984/17/9/024

Characterizing the phases of Langmuir monolayers of cylindrical brushes with x-ray reflectivity and diffraction

Heiko Ahrens[1], **Georg Papastavrou**[1,2] **and Christiane A Helm**[1]

[1] Institut für Physik, Ernst-Moritz-Arndt Universität, Friedrich–Ludwig-Jahn-Straße 16, D-17487 Greifswald, Germany
[2] Department of Chemistry, University of Geneva, 30 Quai Ernest Ansermet, CH-1211 Geneva 4, Switzerland

Received 24 November 2004
Published 18 February 2005
Online at stacks.iop.org/JPhysCM/17/S685

Abstract

Langmuir monolayers of polymacromonomers (cylindrical brushes) with poly(vinyl)pyridine side chains of different length, polyPVP$_{20.8}$ and polyPVP$_{46.7}$, are studied at the air–water interface by means of x-ray diffraction and reflectivity. The advantages of measurements on an aqueous subphase, which contains NaI, are demonstrated. This subphase does not affect the structure of an uncharged monolayer, although NaI is incorporated into the side chains, it provides an enhanced contrast for the x-ray investigations. A structural transition from aligned single molecules to a homogeneous monolayer is found, which is attributed to intra- and intermolecular interactions.

1. Motivation

Miniaturization of devices and control of interfacial properties are drawing modern research towards nanoscopic objects and low-dimensional systems such as single molecules and molecular layers. Particular attention is given to the possibility of actively controlling the domain morphologies in view of possible technological applications. Polymers have proved a promising class of materials for this approach. Surface directed (micro-) phase separation in immiscible polymer systems has been explored extensively. It has been realized that the complex interplay between wetting and phase separation may severely influence the phase separation process, thereby leading to near-surface domain structures, which differ distinctly from the respective bulk morphologies (Elbs *et al* 1999, Krausch 1995). Diblock copolymers consisting of immiscible blocks allow the fine-tuning of the segmental interactions. Actually, segregation of block copolymers on the molecular scale (5–100 nm) can produce astonishingly complex nanostructures (Fasolka and Mayes 2001). The dimensions and lateral density of the patterned morphology are determined by segmental interactions and the copolymer molecular weight. How far the pattern extends in the lateral and thickness directions depends both

on the molecules employed, and on the particular structure of the surface microphase. For diblock copolymers, different microphases occur as a function of the interaction parameter, χ, molecular weight, N, and volume fraction, f (Bates 1991). These microphases are characterized by fluidlike disorder on the molecular scale and a high degree of order at longer length scale (5–100 nm).

Of special interest are the molecular mechanisms of the macroscopic processes, which take place in polymer films at interfaces. On a macroscopic scale, crystallization, wetting, and a wealth of patterned morphologies have been described. If one considers the nanoscopic scale, obviously swelling and conformational changes occur, influenced by the forces from the two planar interfaces as well as intra- and intermolecular interactions. We are particularly interested in elucidating the molecular mechanisms governing nanoscale morphology formation in molecular thin films, especially in aqueous systems.

More complex polymer architectures than linear chains are star or comb polymers, which have been investigated in recent years. Actually, dendrimers and certain extremely branched polymers (i.e. hyperbranched polymers) represent new areas of polymer chemistry. These systems have in common that the polymer conformation can no longer be described as a random coil. Instead, the conformation is determined by the complex architecture, and short-ranged intramolecular interactions. An especially intriguing example consists of cylindrical brushes (Dziezok *et al* 1997). They represent regular comblike polymers with densely grafted side chains. In solution, they adopt a cylindrical conformation, since the main chain is much longer than the side chains and the repulsive interaction between the side chains is sufficiently high. We investigate how the directional persistence of cylindrical brushes changes, if confined to two dimensions, and how adsorption of the side chains to a surface influences the overall molecular conformation (Ahrens *et al* 2004b).

Additionally, we want to address the influence of preferential interfacial adsorption on the film structure by employing cylindrical brushes with statistical mixtures of chemically different side chains. The cylinder conformation is difficult to predict since not only the boundary forces but also the intracylindrical forces are affected by the side chain mixture. On a solid substrate, these statistical copolymacromonomers are no longer stretched cylinders, but form horseshoe- and meanderlike structures (Stephan *et al* 2002).

Due to the defined variability of parameters, especially the area per macromonomer, Langmuir-type monolayers at the air/water interfaces are especially well suited to address the parameters influencing surface morphology. The system provides the additional advantage that surface energies can be directly assessed via surface tension measurements. Furthermore, monolayer equilibrium conformation is established in a much shorter time than on solid substrates. This technique has recently gained increased attention since the last two decades have seen a wealth of new technical developments which allow the study of liquid interfaces at many length scales down to the molecular level (Möhwald 1993, Evans and Wennerström 1994). The x-ray diffraction and reflection technique used here allows for the *in situ* investigation of the aforementioned processes. Thereby information about the structure–properties relationship can be extracted from deformation of single molecules, or even molecular groups adsorbed to an interface (Ahrens *et al* 2000, 2001, Sheiko *et al* 2001).

X-ray and neutron reflectivity measurements have proved most valuable for learning about the segment distribution perpendicular to the water surface. In particular, neutron reflectivity has gained outstanding relevance, since one may deuterate segments completely or partly and thus gain specific contrast (Simister *et al* 1992). However, due to limited flux in neutron scattering experiments one cannot measure at high Q_z-values, as is desirable. Measurement times are too long, and this limits the systematic variation of parameters. X-ray reflection measurements provide an alternative, due to the fact that even laboratory sources provide

sufficient flux and synchrotrons provide ample intensity. However, in most cases scattering relies on electron density contrast, and in this respect many polymers are not sufficiently distinguishable from water. In fortunate cases the two reflectivity methods are complementary (Wesemann *et al* 2003).

To determine the lateral order within the polymeric monolayers, surface sensitive x-ray grazing incidence techniques are suitable. For that scattering geometry, a high flux as supplied by the wiggler beamlines in synchrotrons is necessary. Furthermore, one needs contrast between polymer and solvent.

It has been recently demonstrated that counter ion contrast is a convenient way to achieve that (Ahrens *et al* 1998). The idea is to bind counter ions to the polymer chains in a well defined stoichiometric relationship. Obviously, one has to make sure that the counter ion binding does not change the polymer conformation. While preferential adsorption of a salt molecule or the formation of a charge transfer complex does increase the concentration of counter ions adjacent to the polymer chain, they do not change the persistence length or the medium-ranged interactions which determine polymer conformation. One way to make sure that the ion incorporation does not affect the molecular conformations is to compare the conformations obtained in aqueous salt solutions with those observed in a pure (clean) aqueous subphase.

With polyelectrolytes, i.e. charged polymers, the situation is very different. The charged monomers repel each other, causing an increase in the persistence length (Möhwald *et al* 2004). Furthermore, the counter ions are electrostatically attracted to the polymer chain, leading to a pronounced increase in the local counter ion concentration. In the context of polymeric monolayers, polyelectrolyte brushes have to be mentioned. They have been investigated in depth only in the last few years. Certain features emerge (Netz and Andelman 2003, Zhulina *et al* 1995, Ahrens *et al* 1998): the balance between the entropic and the very strong electrostatic interactions determines the conformation. Theoretically, the decisive question is whether or not the polymer brush length exceeds the Debye length within the polyelectrolyte brush. The Debye length (according to the experiments: 1–10 Å) is a measure of the range of the electrostatic potential surrounding the polymer chains. The thickness of the polymer brush layer is found to be between 100 and 10 000 Å (Balastre *et al* 2002, Ahrens *et al* 1998, Ballauff 2003), i.e. it exceeds the Debye length. Therefore, the counter ions neutralizing the potential along the polyelectrolyte chain are incorporated in the polymer brush. The counter ion concentration may exceed the ion concentration in the subphase by one to four orders of magnitude, leading to a feasible osmotic pressure of the counter ions within the brush. To reduce the osmotic pressure somewhat, the polyelectrolyte brush in the so-called 'osmotic brush phase' is extremely stretched (30–70% of the contour length has been reported repeatedly) (Balastre *et al* 2002, Ahrens *et al* 1998, Ballauff 2003). Detailed theoretical calculations show that the thickness of the osmotically swollen brush changes only very weakly with the grafting density (Netz and Andelman 2003), a prediction which is confirmed by experiments (Ahrens *et al* 2004a). The brush starts to shrink only if the salt concentration in the subphase is similar to the counter ion concentration within the brush. This is the so-called salted brush phase (Ahrens *et al* 1998).

2. Polymacromonomers and copolymacromonomers

Langmuir–Blodgett films at the air/water interface have been studied. These monolayers were formed by cylindrical brushes with a poly(methacrylate) main chain and poly(vinyl)pyridine (PVP) side chains. Iodine incorporates into PVP-brushes (Ahrens *et al* 2004b). Preferential adsorption of NaI to the PVP-brush may occur, or the formation of I^- may lead to charge transfer complexes which increase the concentration of iodine within the brush (Beer *et al* 1997). Poly(vinyl)pyridine adsorbs onto the water surface even though it swells to a certain

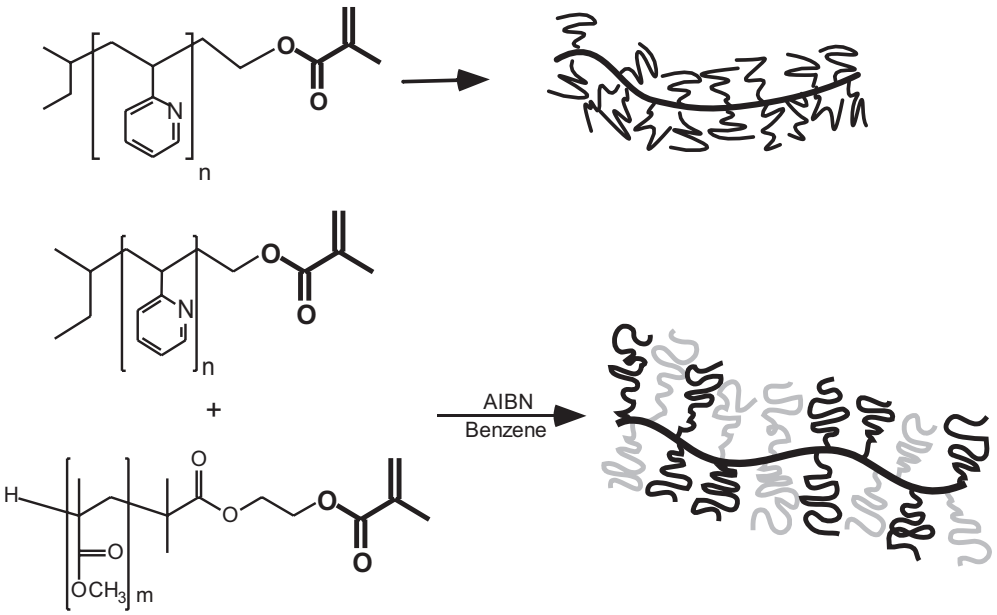

Scheme 1. Top: structural formulae of the cylindrical brushes polyPVP$_{20.8}$ and polyPVP$_{46.7}$ obtained by polymerization of the macromonomers PVP$_{20.8}$ and PVP$_{46.7}$. The contour length of the backbone exceeds one of the side chains by about a factor of five to ten. Bottom: cylindrical brushes poly(QPVP$_{46.7}$)$_{78}$(PMMA$_{35}$)$_{22}$ consisting of QPVP (50% quaternized PVP) and PMMA side chains.

degree (Ahrens *et al* 1999). The high one-dimensional anchoring density ($1/2.5$ Å^{-1}) results in a large side chain volume density close to the backbone. Therefore the conformational freedom of the side chains is reduced adjacent to the backbone. However, the side chain density decreases with increasing distance from the backbone, which suggests an influence of the side chain length on the shape and visco-elastic properties of the mesoscopic cylinders as a whole. Therefore, we investigate polymacromonomers with different side chain lengths, polyPVP$_{20.8}$ and polyPVP$_{46.7}$ (polyPVP$_{46.7}$ with average length 1000 Å, polyPVP$_{20.8}$ with average length 470 Å, and polydispersity ≈2.5; see scheme 1).

With the aim of controlling the interfacial ordering, cylindrical brushes consisting of a statistical mixture of chemically different side chains were prepared: charged QPVP$_{46.7}$ (PVP$_{46.7}$, 50% quaternization by ethyl bromide) and poly(methacrylate) (PMMA$_{35}$) (Stephan *et al* 2002, Dziezok *et al* 1997) (see scheme 1). An average side chain of poly(QPVP$_{46.7}$)$_{78}$(PMMA$_{35}$)$_{22}$ consists of 27.3 MMA monomers and 10.3 VP monomers, 5 of which are quaternized. This results in 2263 electrons per average side chain. Hydrophobic PMMA is not soluble in water. However, QPVP$_{46.7}$ is charged, and thus soluble in water. Therefore, one may expect preferential orientation of PMMA towards air, and of QPVP$_{46.7}$ towards water.

3. Results and discussion

3.1. X-ray reflectivity of polyPVP$_{46.7}$ and polyPVP$_{20.8}$

Figure 1 shows the x-ray reflectivity R/R_F of a polyPVP$_{46.7}$ monolayer with 0.01 M NaI in the subphase and on pure water as a function of the scattering vector Q_z perpendicular to the water surface. Q_z is given by $Q_z = \frac{4\pi}{\lambda} \sin\alpha$ with $\alpha =$ incidence angle and the wavelength λ.

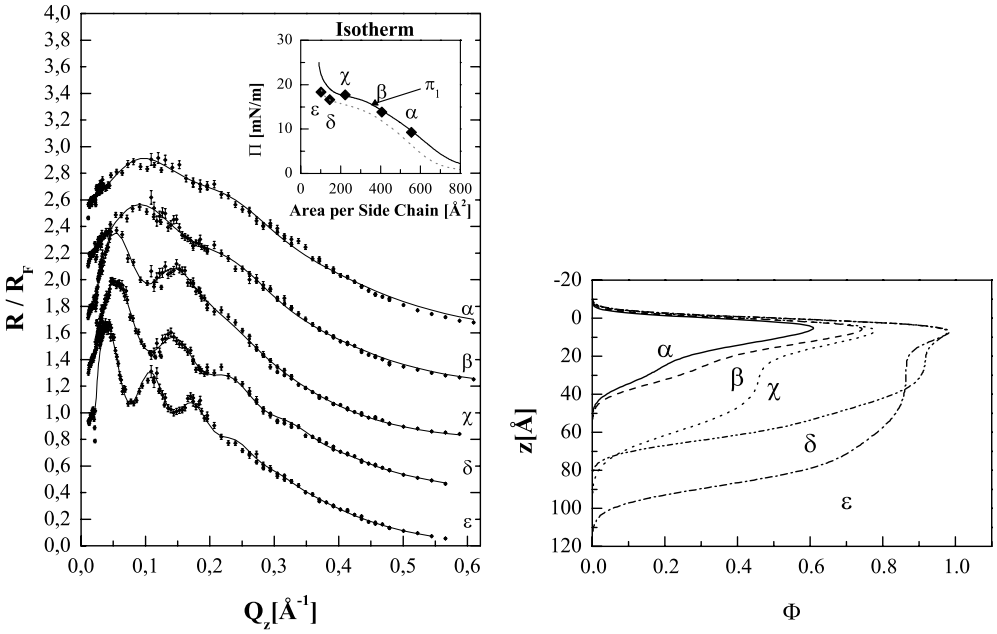

Figure 1. Left: polyPVP$_{46.7}$ monolayers on 0.01 mol l^{-1} NaI (α, β, χ) and on water (δ, ε): (a) normalized x-ray reflectivity R/R_{F} versus vertical scattering vector Q_z. The measurements are displaced vertically by 0.4 units and correspond to the surface pressures indicated ($\alpha, \beta, \chi, \delta, \varepsilon$) in the inset. The dotted isotherm is measured on a clean water subphase, the other on the NaI subphase. Right: best-fit polymer volume fraction $\phi(z)$ corresponding to the data shown on the left. The air–water interface is set to $z = 0$.

The reflectivity R divided by the reflectivity R_{F} expected for an infinitely sharp interface is given according to (Pershan and Als-Nielsen 1984).

$$\frac{R(Q_z)}{R_{\mathrm{F}}(Q_z)} = \left| \frac{1}{\rho_{\mathrm{sub}}} \int \frac{\mathrm{d}\rho(z)}{\mathrm{d}z} \mathrm{e}^{\mathrm{i}Q_z \cdot z}\, \mathrm{d}z \right|^2 . \tag{1}$$

The electron density profile $\rho(z)$ has to be derived from the reflectivity curves by means of models. A successful strategy is to represent the monolayer as a stack of slabs, each with a constant density ρ_i and thickness l_i. The constant density of the semi-infinite subphase has to be added below the interface. Finally, the electron density in the model must be smeared out in the z-direction to account for the intrinsic vertical roughness or diffusivity of the interfaces. The rms roughness, σ, is normally of the order of 3 Å and stems mainly from thermally excited capillary waves on the water surface. The rather large value ($\sigma \approx 3$ Å) means that in the atomic model of $\rho(z)$ it is not necessary to use accurate charge densities of the atoms. As long as each atom contributes its proper charge Z_i the description will be adequate. The large value of σ is also the reason that a slab model may adequately represent the monolayer.

X-ray reflectivity measurements up to $Q_z = 0.4$ Å^{-1} were performed with a home-built set-up described elsewhere (Baltes *et al* 1996). For higher Q_z-values additional measurements were performed at the synchrotron beamline BW1 (HASYLAB, DESY, Hamburg) with the liquid surface diffractometer. Of course one has to verify that the structure is not changed ion specifically. This was done by comparing pressure/area isotherms with NaI and clean water at different ion concentrations in the subphase and also comparing x-ray reflectivity as far as it was possible to obtain reflectivity data without the additional contrast provided by I$^-$ ions.

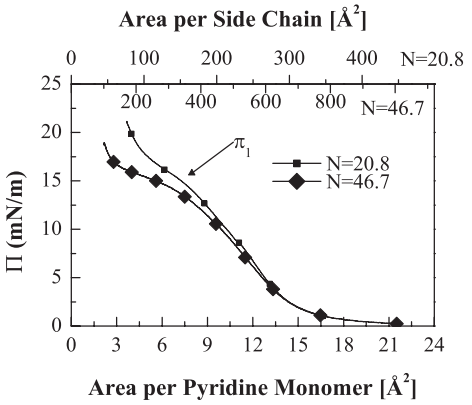

Figure 2. Isotherms of polyPVP$_{20.8}$ and polyPVP$_{46.7}$, normalized per pyridine monomer (bottom x-axis). Along the top x-axis, the area per side chain monomer for the respective polymacromonomers is displayed.

Both isotherms (i.e. with and without NaI) for polyPVP$_{46.7}$ in the inset of figure 1 show a phase transition at the same lateral pressure π_1. The adsorption of PVP to the air/water interface seems to play a crucial role for the expanded phase. Comparing the isotherms of polyPVP$_{20.8}$ and polyPVP$_{46.7}$ (see figure 2), the isotherms of the two different polymacromonomers almost superimpose if they are both normalized with respect to the area per pyridine monomer. Nonzero pressure occurs at 17 Å^2/pyridine, and at 7.5 Å^2/pyridine ($\pi_1 \approx 15$ mN m^{-1}) the pronounced change in slope indicates a phase transition (Albrecht *et al* 1978).

Figure 1 shows the x-ray reflectivity curves along the isotherm. The detailed analysis of the curves, i.e. the parameters for all slabs to fit the reflectivity curves, is described in Ahrens *et al* (2004b). For large macromonomer areas, the subphase contains 0.01 mol l^{-1} NaI. The iodine addition improves the contrast, and therefore two interference maxima can be observed, even for high macromonomer areas (curves α, β, χ). Upon monolayer compression the maxima shift to smaller Q_z-values, indicating film thickening. Also up to two more interference maxima appear. Detailed analysis reveals that the interference extrema are equidistant (except for the most compressed curves δ and ε). From these fast oscillations the total film thickness can be deduced. The centres of these oscillations constitute a very broad maximum, corresponding to a slow oscillation. To accommodate that, a thin yet high-density slab at the air-side is necessary. In total, two slabs for the α, β and γ curves (three slabs for the δ and ε curves) are necessary to simulate the electron density profile of the monolayer. One obtains for the roughness of the monolayer/air interface a value of $\sigma_{\text{air}} = 3$–4 Å, which is significantly smaller than 6–9 Å for the monolayer/water interfaces (see figure 1).

The monolayer electron density on the NaI subphase appears to be larger than on pure water, suggesting I^- incorporation. Both the amount of water molecules n_{H_2O} and iodine ions n_I per macromonomer are calculated according to

$$V = A \sum_i l_i = n_P V_P + n_I V_I + n_{H_2O} V_{H_2O} \tag{2}$$

$$E = A \sum_i \rho_i l_i = n_P E_P + n_I E_I + n_{H_2O} E_{H_2O} \tag{3}$$

where A is the area per macromonomer, $V_P = 146$ Å^3, $V_I = 58.1$ Å^3, and $V_{H_2O} = 146$ Å^3 are the molecular volumes of a pyridine monomer, an iodine ion, and a water molecule,

respectively. E_P, E_I, and E_{H_2O} are the corresponding numbers of electrons. $n_P = 46.7$ is the degree of polymerization per side chain. E signifies the number of all the electrons in the cylindrical brush per macromonomer, and V is the respective volume (ρ_i and l_i symbolize the electron density and the thickness of the slab i). For large macromonomer areas, the side chains are swollen. On compression, the swelling decreases and eventually we find for n_{H_2O} 1.58 water molecules per pyridine monomer, almost the same value as for polyPVP$_{20.8}$ (Ahrens *et al* 1999). n_I is found to be constant; it is equal to 5.8 iodines per macromonomer.

To compare the segment density profiles of polyPVP$_{46.7}$ obtained at different molecular areas, the volume fraction profile of the polymer is calculated according to

$$\Phi(z) = \frac{\rho(z) - \rho_{sub}\,\mathrm{erf}(z/\sigma_{air})}{\rho_{pol} - \rho_{sub}} \tag{4}$$

where $\rho(z)$ is the measured electron density from the reflectivity curves, and $\rho_{sub} = 0.334\,\mathrm{e\,\AA^{-3}}$ is the electron density of the subphase. ρ_{pol} is the electron density of either a hydrated macromonomer or a hydrated macromonomer and the appropriate amount of iodine, i.e. 0.12 iodines per pyridine monomer. The error function accounts for the roughness at the liquid/gaseous interface, which is set at $z = 0$. Obviously, the molecules in the monolayer do not maintain their circular cross-section. At large molecular areas, a cylindrical brush is very flat, with most side chains adsorbed to the air–water interface. By reducing the area per side chain from 555 to 100 Å^2, the thickness of the monolayer can be increased by a factor 3, up to 88 Å. Always, some PVP side chains are flatly adsorbed to the liquid–gas interface.

The first indication for the existence of a phase transition at π_1 was obtained from polyPVP$_{20.8}$ monolayers, which were transferred at selected areas per side chain onto a solid substrate (Ahrens *et al* 1999). Aligned single molecules (see figure 3) are observed by AFM, if an expanded monolayer is imaged. Beyond the phase transition at π_1, the transferred monolayer appears instead totally homogeneous on the AFM images.

Also, the volume density profiles of the cylindrical brushes in the expanded phase are very similar, with pronounced side chain adsorption to the air/water interface (see figure 3). However, in the compressed state, i.e. beyond the phase transition at π_1, there are unambiguous structural differences between polyPVP$_{46.7}$ and polyPVP$_{20.8}$ (Ahrens *et al* 2004b). The highest density of polyPVP$_{46.7}$ is found at the air/polymer interface, which can be attributed to preferential adsorption of the side-chains (see figures 1 and 3). The cylinder backbone cannot be identified within the polymer density profile. Apparently, the polymacromonomer backbones are not confined to the interface, but are vertically distributed within the monolayer. In contrast, for polyPVP$_{20.8}$, the most dense slab is attributed to the cylinder backbone; it is sandwiched between two less dense slabs (of equal thickness and density) containing side chains only, as was found with reflectivity measurements published earlier (Ahrens *et al* 1999) (see figure 3). For polyPVP$_{46.7}$, no preferential adsorption to the air/water interface is found. These differences in the compressed phase can be attributed to the increased configurational freedom expected for longer side chains.

3.2. X-ray diffraction of polyPVP$_{46.7}$ and polyPVP$_{20.8}$

The ordered phase as observed after transfer to solid substrates can also be examined *in situ* at the air/liquid interface by x-ray diffraction (Ahrens *et al* 2004b). In the case of ordered arrangements x-ray diffraction is known to be the most direct and precise technique of structure analysis. These measurements became possible also for the liquid/gaseous interface in the last 15 years by making use of the high brilliance of synchrotron sources (Kjaer *et al* 1987). With this technique an x-ray beam strikes the surface at grazing incidence (grazing incidence

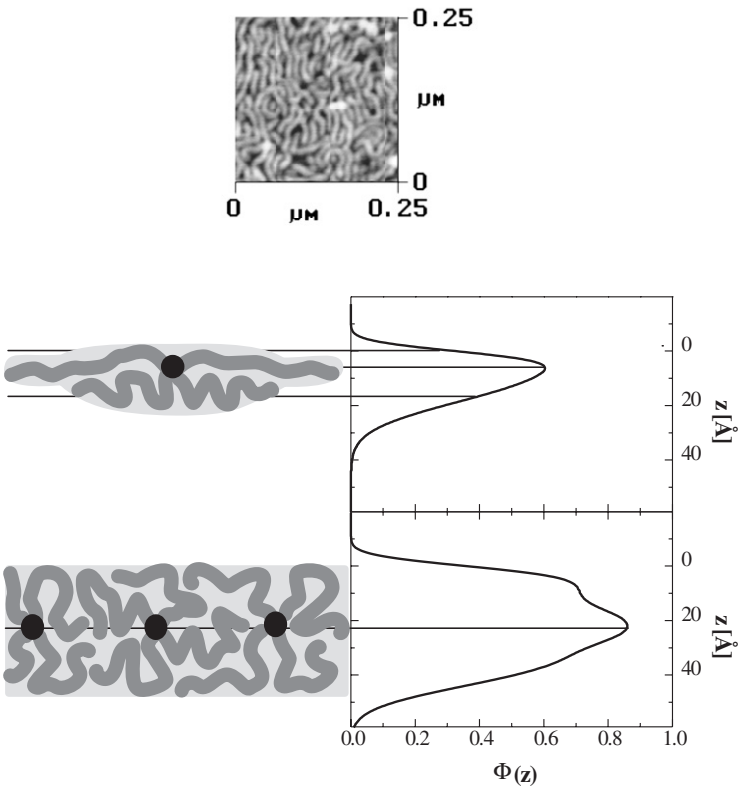

Figure 3. Top: AFM image of a polyPVP$_{20.8}$ monolayer transferred at a molecular area of ≈250 Å^2/macromonomer. After compressing beyond the phase transition at π_1, i.e. at molecular areas below ≈160 Å^2/macromonomer, it was impossible to observe any pattern (Ahrens *et al* 1999). Centre and bottom: electron density profile of polyPVP$_{20.8}$ as derived from x-ray reflectivity curves, together with a schematic drawing of cylindrical brush cross-section (centre 232 Å^2/macromonomer, bottom 101 Å^2/macromonomer). The latter is consistent both with the reflectivity results in Ahrens *et al* (1999) and with the GID findings described in figures 5 and 6.

diffraction, GID), and assuming lateral periodicity of the atom density projected on the surface, one observes Bragg peaks. The scattered intensity $I(\boldsymbol{Q})$ is measured as a function of the scattering vector $\boldsymbol{Q} = (Q_x, Q_y, Q_z) = (\boldsymbol{Q}_{xy}, Q_z)$, with $\boldsymbol{Q}_{xy}$ as the horizontal and Q_z as the vertical scattering vector. There is no restriction on the z-component of the Bragg scattered ray. A 2D crystalline lattice confines the x-ray scattering vector to Bragg rods along the z-direction, not to Bragg points as in the case of a 3D crystal.

The horizontal and vertical components of the scattering vector $\boldsymbol{Q}$ are

$$Q_{xy} = \frac{2\pi}{\lambda}\sqrt{\cos^2\alpha_\mathrm{i} + \cos^2\alpha_\mathrm{f} - 2\cos\alpha_\mathrm{i}\cos\alpha_\mathrm{f}\sin 2\theta_{x,y}} \tag{5}$$

$$Q_z = \frac{2\pi}{\lambda}(\sin\alpha_\mathrm{i} + \sin\alpha_\mathrm{f}) \tag{6}$$

where α_i and α_f are the angles between the plane of the liquid surface and the incident and the diffracted beams, respectively, and $2\theta_{x,y}$ is the angle between the incident and diffracted beams projected onto the horizontal (x, y) plane. The Q_{xy} positions of the Bragg peaks yield

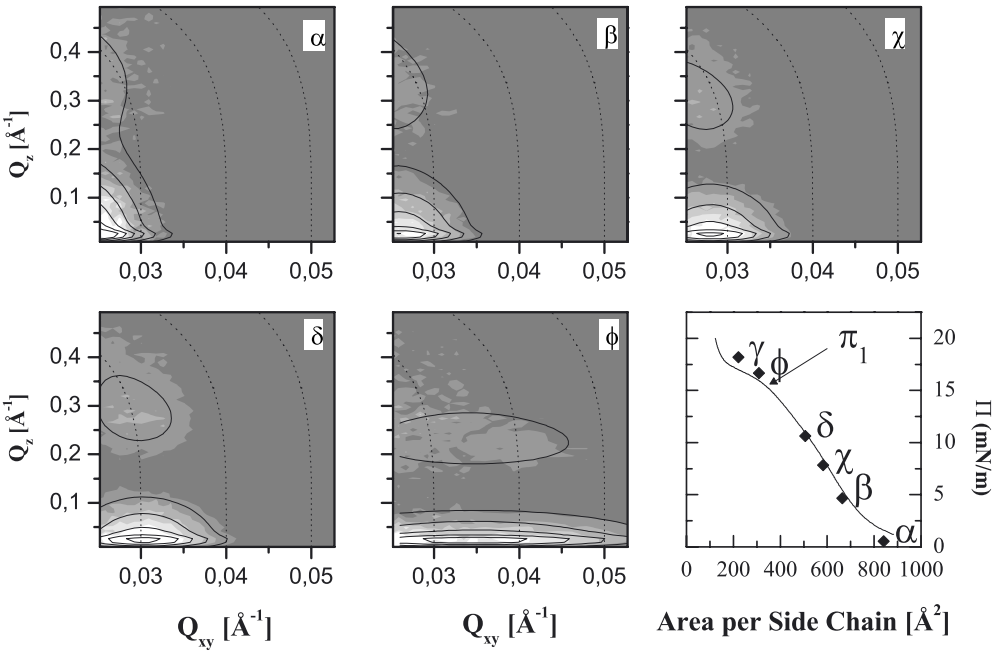

Figure 4. Left: diffracted intensity for polyPVP$_{46.7}$ monolayers on 0.01 mol l^{-1} NaI (contour plots, au) in the Q_{xy}–Q_z plane. The slightly bent vertical lines indicate constant Q_{xy}. The measurements correspond to the surface pressures indicated (α, β, ...) in the isotherm. Lines indicate fits to the model described in the text. At γ, no peak was found. The phase transition as observed in the isotherm is indicated by π_1.

the lattice repeat distances

$$d = \frac{2\pi}{Q^{hk}} \tag{7}$$

which can be indexed by two indices (h, k) to yield the unit cell ($Q_{xy} = Q^{h,k}$), assuming no periodicity in the z-direction results in a scattering which is concentrated along rods in reciprocal space. The measured intensity in the z-direction is therefore only given by the molecular form factor

$$I_{h,k}(Q_z) \propto \left|F_{h,k}(Q_z)\right|^2. \tag{8}$$

Because the signal is obtained by averaging over many randomly distributed domains one basically observes a two-dimensional powder pattern.

As an example, figure 4 compares contour plots measured for polyPVP$_{46.7}$ at different pressures. In the expanded phase, both the first and second maxima of the rod scan are observed. One occurs at $Q_{z,1} = 0$ and the other at larger Q_z. Upon further compression of the monolayer, the rod scans shift to larger Q_{xy}-values, indicative of a decrease of the lattice spacing (see figure 5(a)). Compressing slowly beyond π_1, the peaks disappear. Approaching π_1, additionally the peak width ΔQ_{xy} increases, indicating a decrease in correlation length ξ, which is calculated according to $\xi = \frac{1.6\pi}{\mathrm{fwhm}(Q^{hk})}$ (the peaks in Q_{xy} are fitted to Gaussians, thus the full width at half maximum, fwhm, is determined (Kjaer *et al* 1991)).

Assuming that the diameter of the flattened cylinder corresponds to the cylinder backbone separation we developed a simple model: the side chains are aligned perpendicularly to the backbone and in the case of no lateral interaction they are completely stretched. Side chain

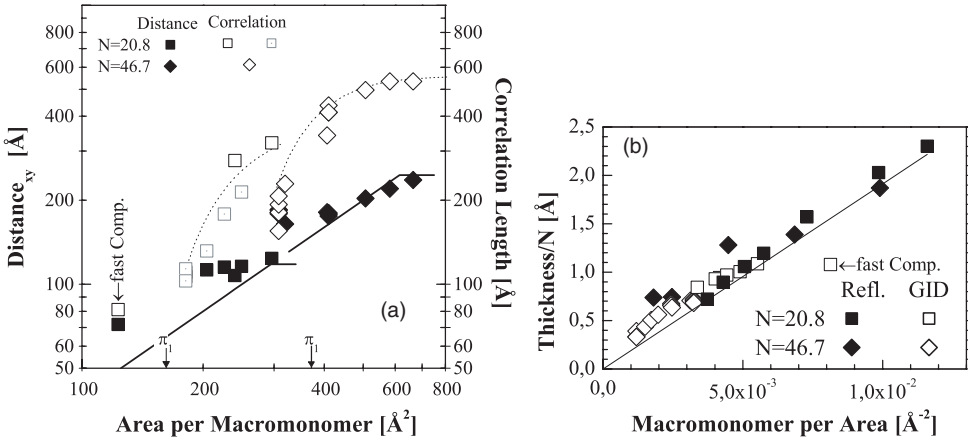

Figure 5. (a) Lattice spacing 'Distance$_{xy}$' and correlation length ξ for both polymacromonomers investigated. The phase transition as observed in the isotherm is indicated by π_1. (b) The thickness l of the ordered monolayer is normalized with respect to the degree of side chain polymerization, as determined from GID (open symbols) and from reflectivity data (solid symbols). Dotted curves in (a) are guides to the eye. Straight lines in (a) and (b) were calculated assuming constant cylinder volume.

deformation and desorption sets in when the monolayer is compressed. Then, the cylinder diameter $2r$ is calculated from the side chain area A measured with the isotherm according to $2r = 2A/a$ (every $a = 2.5$ Å is a side chain with a contour length of $r_{\max} = 123$ Å attached to the cylinder backbone. For polyPVP$_{20.8}$, $r_{\max} = 59$ Å). Experimentally, we find that the cylinder backbone separation corresponds at most to twice the contour length of the PVP side chains. On monolayer compression, the cylinder diameter decreases linearly with the area per side chain, from 250 to 180 Å. This decrease is less than predicted by our simple model (see figure 5(a)). The deviations can be attributed to defect annealing, which occurs during the further monolayer compression.

The peaks in Q_{xy} are easier to quantify than the rod scans, i.e. the peaks in Q_z. The intensity of a Bragg rod at a particular Q_z-value is determined by the square of the molecular structure factor $|F_{\mathrm{mol}}(Q_z)|^2$, see equation (6). For small molecules, $|F_{\mathrm{mol}}(Q_z)|^2$ is evaluated according to an atomic coordinate model of the molecules. Obviously, mesoscopic worms with a locally random side chain configuration cannot be described as laterally incompressible atoms or pseudoatoms consisting of groups of atoms. By using a much coarser model of the average molecular structure in the unit cell, a laterally periodic electron density profile can be derived (Ahrens *et al* 2004b).

For a planar monolayer on a smooth substrate, the electron density $\rho_{\mathrm{total}}(\boldsymbol{r})$ can be divided into a laterally homogeneous part, $\rho(z)$ (known from x-ray reflectivity measurements), and its local deviation $\rho_{\mathrm{diff}}(x, y, z)$ (with $\int\int \mathrm{d}x\,\mathrm{d}y\,\rho_{\mathrm{diff}}(x, y, z) = 0$), resulting in

$$\rho_{\mathrm{total}}(\boldsymbol{r}) = \rho(z) + \rho_{\mathrm{diff}}(x, y, z). \tag{9}$$

Thus, one obtains for the structure factor

$$|F_{\mathrm{mol}}(Q_z)|^2 = \left| \int \mathrm{d}z \exp(\mathrm{i}Q_z z)\tilde{\rho}(z) \right|^2 \tag{10}$$

where $\tilde{\rho}(z)$ is the Fourier transform of the lateral electron density variation,

$$\tilde{\rho}(z) = \int\int \mathrm{d}x\,\mathrm{d}y \exp(\mathrm{i}(Q_x \cdot x + Q_y \cdot y))\rho_{\mathrm{diff}}(x, y, z). \tag{11}$$

In the simplest case, the monolayer consists only of one laterally structured layer. However, this leads to contradictions, concerning both the intensity (too high) and the position (too low) of the second maximum observed in the rod scan, $Q_{z,2}$.

Actually, a pronounced minimum in the Fourier transform of the lateral electron density variation $\tilde{\rho}(Q_{xy}, z)$ is necessary to obtain such an intense second maximum in the rod scan. Reflectivity measurements of the expanded phase indicate the existence of a plane where the deformed cylinders touch. This plane can be identified with the surface plane covered with adsorbed side chains (see figures 1 and 3). Above and below that contrast-free plane the electron density has to be laterally periodic, a feature that can be approximated by two Gaussian peaks in $\tilde{\rho}(z)$. These two Gaussians, separated by a distance L, are characterized by their widths w_1 and w_2, and intensities A_1 and A_2. The maximum lateral density variation occurs inside the monolayer and vanishes at the interfaces to the subphase and the air, respectively. To obtain the monolayer thickness l^*, it is necessary to include the hwhm (half width half maximum) of the peaks $l^* = L + w_1 + w_2$. The thus determined monolayer thickness l^* is in good agreement with the results from x-ray reflectivity (see figure 5(b)), for both polymacromonomers investigated.

The lateral structure exhibits a periodicity of width d (see figures 5 and 6), consisting of a polymer stripe with vertically varying width $D(z)$ and electron density ρ_1 and another stripe of width $d - D(z)$ with electron density ρ_2. Because $\int\int \mathrm{d}x\,\mathrm{d}y\,\rho_{\mathrm{diff}}(x, y, z) = 0$ the following conditions have to be fulfilled:

$$D\rho_2 - (d - D)\rho_1 = 0 \tag{12}$$

and

$$\rho_1 - \rho_2 = \rho_{\mathrm{Polymer}} - \rho_{\mathrm{Surroundings}}. \tag{13}$$

Assuming that the stripes are aligned in the y-direction, one obtains for $\tilde{\rho}(z_i)$

$$\begin{aligned}\tilde{\rho}(z_i) &= \rho_1 \int_{-D/2}^{D/2} \exp(\mathrm{i}Q_x \cdot x)\,\mathrm{d}x \\ &\quad + \rho_2 \left(\int_{-d/2}^{-d/2+D/2} \exp(\mathrm{i}Q_x \cdot x)\,\mathrm{d}x + \int_{D/2}^{d/2-D/2} \exp(\mathrm{i}Q_x \cdot x)\,\mathrm{d}x \right) \\ &= \frac{(\rho_1 - \rho_2)\sin(Q_x \cdot D(z)/2)}{Q_x} \\ &= \frac{d(\rho_1 - \rho_2)}{2\pi} \sin[\pi \cdot D(z)/d] \qquad \text{because of } Q_x = Q^{h,k} = 2\pi/d. \end{aligned} \tag{14}$$

Note that the peaks in the rod scan are largest at z_1, when $2D(z_1) = d$. Also, a large value of the local electron density difference, $\rho_1 - \rho_2$, helps. To validate this model, $\tilde{\rho}(Q_{xy}, z)$ is calculated from the volume fraction $\Phi(z)$ (see equation (4)) at a molecular area of 406 Å^2, a molecular area where both very structured x-ray reflectivity and GID measurements are available. The thus obtained Fourier transformed lateral density variation is to be compared to the two Gaussians obtained empirically by performing a least square fit of the GID data to equation (15).

$$|F_{\mathrm{mol}}(Q_z)|^2 \propto A_1^2 w_1^2 \mathrm{e}^{-Q_z^2 w_1^2} + A_2^2 w_2^2 \mathrm{e}^{-Q_z^2 w_2^2} + 2A_1 A_2 w_1 w_2 \mathrm{e}^{-\frac{Q_z^2(w_1^2+w_2^2)}{2}} \cos(Q_z L) \tag{15}$$

which is derived from

$$\tilde{\rho}(Q_{xy}, z) = A_1 \mathrm{e}^{-\frac{(z-L/2)^2}{2w_1^2}} + A_2 \mathrm{e}^{-\frac{(z+L/2)^2}{2w_2^2}}. \tag{16}$$

The following additional assumptions are used: ρ_{pol} is assumed to be constant, with a hydration of 1.58 water molecules per pyridine monomer, consistent with the reflectivity data; see figures 1 and 3, and equations (2)–(4). Above the maximum of $\Phi(z) = \Phi(z_{\max})$, i.e. above

the PVP adsorption layer, we have $\rho_{\text{Surroundings}} = \rho_{\text{air}} = 0$, while below the maximum, the monolayer is immersed in water, i.e. $\rho_{\text{Surroundings}} = \rho_{\text{sub}} = 0.334\,\text{e}^-\,\text{Å}^{-3}$. Thanks to the iodine incorporation, one has $\rho_{\text{pol}} = 0.406\,\text{e}^-\,\text{Å}^{-3}$, which exceeds $\rho_{\text{sub}} = 0.334\,\text{e}^-\,\text{Å}^{-3}$ substantially. Without iodine, one would have $\rho_{\text{pol}} = 0.385\,\text{e}^-\,\text{Å}^{-3}$, which provides only very weak second maxima in the rod scans.

The minimum in $\tilde{\rho}(Q_{xy}, z)$ derived from the rod scans is obtained only after multiplying $\Phi(z)$ from the reflectivity data by a factor of 1.4 to obtain a close-packed adsorption layer. Focusing on an ordered domain, the increased polymer density in the adsorption layer is justified because only aligned single molecules contribute to the GID signal, when the alignment is defect-free. Considering the whole film, both the AFM images (see figure 3) and the rather low compressibility observed in GID suggest an extremely high defect density, which decreases the average density in the adsorption layer.

The cross-section of the deformed cylinders as obtained from $\tilde{\rho}(Q_{xy}, z)$ is depicted in figure 6, which also shows both the volume fraction and the Fourier-transformed lateral electron density variation. The strong and narrow maximum of $\tilde{\rho}(Q_{xy}, z)$ on top of the adsorption layer can be attributed to the cylinder backbones protruding slightly out of the water. The difference in electron density of polymer and air is dramatic; therefore the peak in $\tilde{\rho}(Q_{xy}, z)$ is intense and narrow. In contrast, the peak due to the molecule/subphase interface is rather broad and weak. These features are attributed to the vertically extended side chains directly beneath the backbone and to the small difference in the electron density provided by polymer and water. Since the monolayer is laterally structured beneath the adsorption layer, it is likely that the side chains are either desorbed or adsorbed, but never partially desorbed.

Note that the structural roughness provided by the curved cylinder surface does not contribute to the water/air roughness as measured with x-ray reflectivity, because the amplitude of the surface corrugation is about 1 Å, and its wavelength is a few 100 Å. The surface roughness as observed with x-ray reflectivity is determined by capillary waves, and long wavelengths (μm to mm, depending on the slit configuration) with their large amplitude contributing the most (Schwartz *et al* 1990).

Above the phase transition, the isotherms exhibit a very large compressibility. In this regime no lateral order could be detected. Obviously the side chains of different molecules mix. This results in a homogeneous monolayer whose thickness increases further upon lateral compression (see figures 1 and 5).

3.3. X-ray reflectivity of poly(QPVP$_{46.7}$)$_{78}$ (PMMA$_{35}$)$_{22}$

In contrast to the PVP macromonomers examined in the previous sections, the side chains of poly(QPVP$_{46.7}$)$_{78}$(PMMA$_{35}$)$_{22}$ exhibit not an entirely neutral character due to the charge in QPVP. The reflectivity curves for this copolymacromonomer on clean water are shown on the left side of figure 7. A pronounced maximum for the reflectivity is already observed at large area per side chain. This maximum shifts upon film compression to smaller Q_z-values, which indicates an increasing thickness of monolayer. The high values of R/R_{F} at the critical angle obtained for all macromolecular areas shown in figure 7 are in strong contrast to reflectivity data obtained from polyPVP$_{46.7}$ and polyPVP$_{20.8}$. A reflectivity curve as depicted in figure 7 is indicative for a thick layer with an increased refractive index compared to the subphase. Indeed, the large R/R_{F}-values are consistent with an extended polymer brush. This assumed model is further supported by the δ curve, where a weak additional maximum at very low Q_z can be recognized.

The electron density profile as shown on the right side of figure 7, was modelled from two slabs for the different macromolecular areas. Within the error margin the thickness of

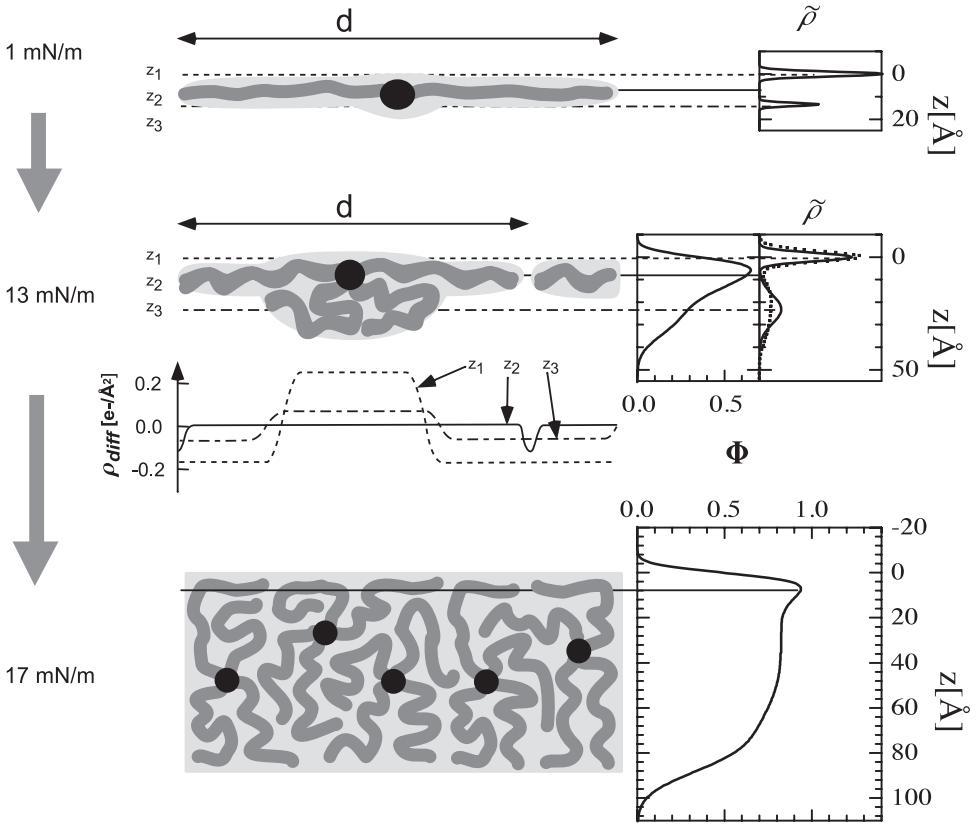

Figure 6. Scheme of a polyPVP$_{46.7}$ monolayer at different molecular areas, together with volume fraction profile Φ, as calculated from electron density profiles (left, see figure 3) and the Fourier transformed lateral electron density variation (Q_{xy}, z), if Bragg peaks could be observed (far right). At the onset of pressure increase (top, molecular area 890 Å^2), the cylinder diameter corresponds to twice the side chain contour length. On compression, yet still in the expanded state (centre, side chain area 406 Å^2), a laterally almost homogeneous adsorption layer exists (at z_2). At this molecular area about half the side chains are adsorbed to the air/water interface, as depicted. The adsorption layer induces a deformed monolayer/air interface (at z_1), and beneath this the polymer coils protrude into the water (at z_3). Both effects result in a laterally periodic electron density (left centre) and provide the contrast for in-plane diffraction. Furthermore, from the volume fraction $\Phi(z)$, $\tilde{\rho}(Q_{xy}, z)$ is calculated with the assumptions described in the text (dashed line). Above the phase transition, at an area per side chain of 350 Å^2, the backbone is vertically distributed and the side chains mix laterally, and no contrast for x-ray diffraction is available (bottom, side chain area 101 Å^2).

both slabs remains almost constant upon compression, exhibiting only an increase in electron density. The first slab can be assigned to an absorption layer, with an approximate thickness of 10–14 Å. Only in the most compressed state (δ) does the thickness of this slab increase to 18 Å. The subsequent slab exhibits a constant thickness of 41 $\pm$ 9 Å and can be assigned to an extended polyelectrolyte brush. Such a constant thickness is indicative of an osmotically swollen phase, well known for polyelectrolyte brushes. The brush length would amount to 33% of the contour length in the case of consisting entirely of PVP (contour length of 123 Å). Such a pronounced stretching is indeed typical (Ahrens *et al* 1998).

The reflectivity measurements in figure 8 were obtained with the same copolymacromonomer poly(QPVP$_{46.7}$)$_{78}$(PMMA$_{35}$)$_{22}$, but in this case the aqueous subphase

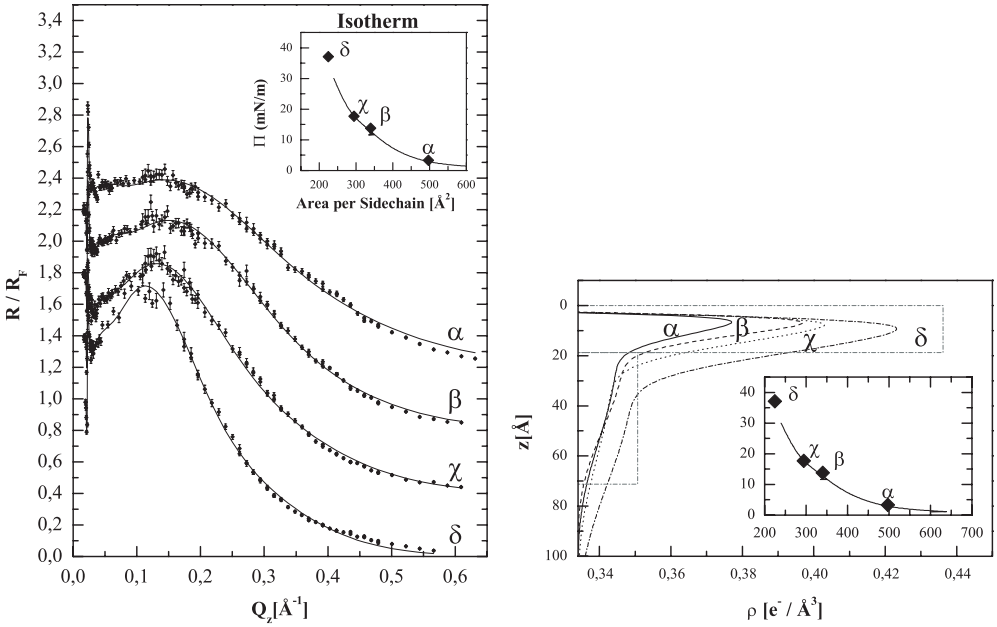

Figure 7. Poly$(QPVP_{46.7})_{78}(PMMA_{35})_{22}$ monolayers on clean water. Left: normalized x-ray reflectivity R/R_F versus vertical scattering vector Q_z. The measurements are displaced vertically by 0.4 units and correspond to the molecular areas indicated (α, β, χ, δ) in the isotherm shown in the inset. Right: best-fit electron density profiles corresponding to the data shown on the left. The air–water interface is set to $z = 0$. For the δ curve the two slabs are shown as dotted lines, from which the electron density profile is calculated.

Table 1. Parameters derived from reflectivity profiles of poly$(QPVP_{46.7})_{78}(PMMA_{35})_{22}$ on water. An average side chain consists of 27.3 MMA monomers and 10.3 VP monomers, 5 of which are quaternized. This results in 2263 electrons per average side chain. The slab with index '1' describes the air adjacent interface. The next slab (index '2') is adjacent to the water. The fits were performed with the constraint that the roughness of the polymer–water interface is $\sigma_{sub} = L_2/2$.

No in figure 7	Area (Å^2)	Pi (mN m^{-1})	L_1 (Å)	ρ_1 (e$^-$ Å^{-3})	L_2 (Å)	ρ_2 (e$^-$ Å^{-3})	σ_{Air} (Å)	$\sigma_{1,2}$ (Å)	Vol (Å^3)	N_{e-}	V_{Pol} (Å^3)
α	497	3.3	10.9	0.389	43.8	0.346	2.6	5.5	27 212	9648	4939
β	340	13.8	11.1	0.417	38.6	0.348	3.0	5.5	16 882	6139	5131
	311	14.6	10.7	0.443	23.9	0.360	3.2	5.3	10 749	4146	4973
χ	294	17.7	14.3	0.420	47.6	0.345	3.2	7.2	18 224	6601	5086
	281	22.5	15.7	0.423	33.8	0.349	3.5	7.5	13 874	5167	5036
	225	35.2	19.6	0.421	44.0	0.349	3.5	8.7	14 301	5307	5044
δ	225	37.1	18.8	0.437	52.5	0.351	3.8	7.9	16 027	5986	4732

contained 10 mM NaI (see figure 8). The resulting reflectivity curves show pronounced differences compared to the ones obtained on the pure water subphase. In addition to the pronounced first maximum a second maximum can be observed upon compression, indicative of a low polymer–water roughness. Also, one does not observe the high intensity at low Q_z-values which would indicate a polyelectrolyte brush. The electron density profiles can be described again with two slabs, of different thicknesses (see table 2). At large side chain areas, an adsorption layer is found. However, on compression the highest electron density, i.e. the largest segment density, is found on the side of the subphase. Obviously a polymer desorption

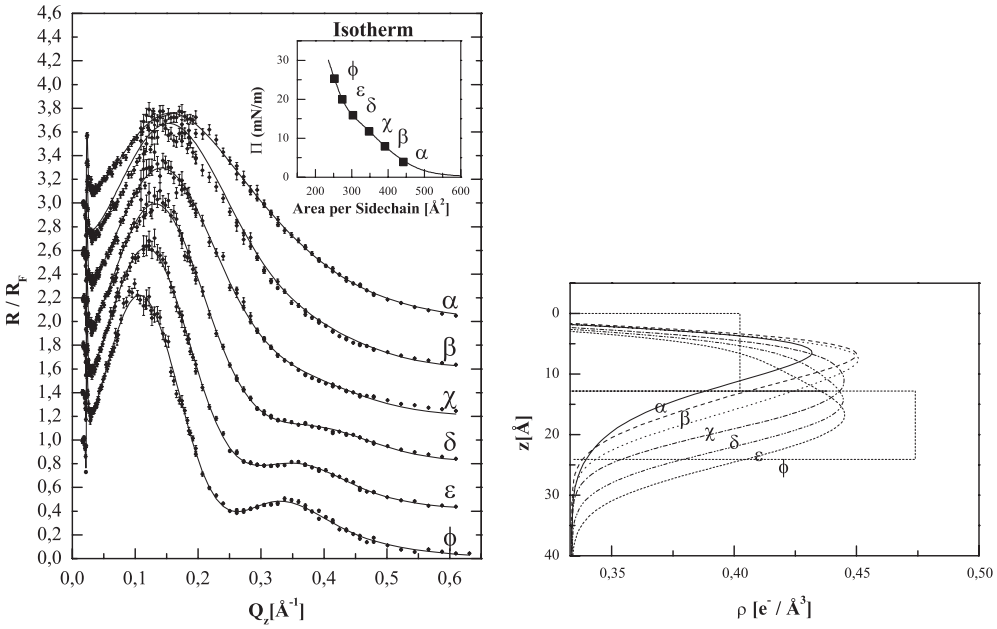

Figure 8. Poly$(PVP_{46.7})_{78}(PMMA_{35})_{22}$ monolayers on 10 mM NaI solution. Left: normalized x-ray reflectivity R/R_F versus vertical scattering vector Q_z. The measurements are displaced vertically by 0.4 units and correspond to the molecular areas indicated in the isotherm shown in the inset. Right: best-fit electron density profiles corresponding to the data shown right. The air–water interface is set to $z = 0$.

Table 2. Parameters derived from reflectivity profiles of poly$(QPVP_{46.7})_{78}(PMMA_{35})_{22}$ on 10 mM NaI. The parameter assignment is identical to table 1. The fits were performed with the following constraints. $\sigma_{1,2} = L_1/2\ \sigma_{sub} = L_2/2$. Additionally, the amount of water molecules, N_{H_2O}, and iodine atoms, N_I, within each average side chain are given.

No in figure 8	Area (Å^2)	Pi (mN m^{-1})	L_1 (Å)	ρ_1 (e$^-$ Å^{-3})	L_2 (Å)	ρ_2 (e$^-$ Å^{-3})	σ_{Air} (Å)	Vol (Å^3)	N_{e-}	N_{H_2O}	N_{Iod}
α	442	3.9	10.4	0.469	L_1	0.357	3.0	9220	3806	130	4.5
	400	6.7	8.3	0.535	11.9	0.368	4.1	8096	3534	87	7.6
β	391	7.9	8.8	0.499	L_1	0.401	3.4	6866	3089	48	6.5
χ	348	11.8	9.2	0.485	L_1	0.425	3.5	6415	2920	34	6.0
δ	303	15.9	9.4	0.437	L_1	0.464	3.2	5702	2570	17	2.6
	275	18.8	8.6	0.405	14.1	0.454	3.2	6254	2722	37	1.7
	275	18.8	10.9	0.416	12.4	0.457	3.3	6413	2807	40	2.7
ε	252	25.3	11.7	0.422	10.3	0.474	3.2	6009	2682	26	2.9
ϕ	442	3.9	12.8	0.403	11.3	0.483	3.1	6073	2675	30	2.1

transition takes place, in contrast to the clean water subphase. No stringent indications of the presence of extended polyelectrolyte brushes can be found in the NaI subphase.

The amount of hydration is low: about one water molecule per monomer. Considering the many hydrophobic MMA monomers, it makes sense that the hydration is slightly lower than the one found for a pyridine monomer in polyPVP.

It seems unlikely that the slab adjacent to the air interface consists solely of PMMA. In the air-adjacent slabs there are not enough electrons and volume to contain all PMMA. At present

there is not even clear evidence that it consists mainly of PMMA. Additional experiments with different side chain compositions, and especially GID experiments, are necessary to address this question. Nevertheless, the present experiments demonstrate the influence of the NaI counter ions on the monolayer film: on the one hand NaI in the subphase advantageously enhances the x-ray contrast of neutral PVP, and on the other hand it can strongly influence the intramolecular forces (and presumably also the intermolecular forces) in the case of charged cylindrical brushes. It should be noted that both effects stem from the iodine incorporation in the polymer brushes. One may conclude that very powerful structural information can be obtained with x-ray methods due to counter ion contrast; however, one has to be very careful to exclude ion specific effects.

4. Conclusion and outlook

Two competing interactions determine the phase behaviour of neutral cylinder brush monolayers: (i) pronounced side chain adsorption to the interface causes backbone stretching and alignment of single molecules; (ii) a vertically diffuse cylinder backbone and laterally homogeneous side chain distribution are entropically more favourable: they induce a homogeneous monolayer. On monolayer compression, side chain desorption occurs and causes a phase transition. The fewer side chains that are adsorbed in the expanded phase, the smaller are the intracylinder forces which cause molecular stretching. The phase transition occurs when the backbone desorbs from the interface, and the side chains from different molecules interpenetrate and mix. Therefore, the phase transition is caused not only by intermolecular interactions as is known from polymers with a simple architecture, but by intramolecular interactions, too. To quantify preferential interfacial adsorption of cylindrical brushes with mixed side chains (some of them charged), the conformation is strongly influenced by the ion content in solution. This phenomenon needs to be further explored.

Acknowledgments

We are deeply grateful to Kristian Kjaer for his continuous help with the liquid surface spectrometer at BW1, especially with the alignment of the slits before the soller and his prompt support with those problems which arise suddenly out of thin air. We thank Tim Stephan and Manfred Schmidt for providing us with the polymer samples. The Langmuir trough with enclosure used during the experiments was a generous loan by Mathias Lösche and Peter Krüger; their help is appreciated. The English of this paper greatly improved, thanks to Neil McTaggart. We thank HASYLAB, DESY (Hamburg, Germany) for synchrotron beamtime at the BW1 line, and support. The financial support of the Schwerpunkt 'Benetzung' (He 1616/9-2,3,4) is gratefully acknowledged, as well as the support of the state Mecklenburg-Vorpommern.

References

Ahrens H, Baekmark T R, Merkel R, Schmitt J, Graf K, Raiteri R and Helm C A 2000 *Chem. Phys. Chem.* **1** 101–6
Ahrens H, Förster S and Helm C A 1998 *Phys. Rev. Lett.* **81** 4172–5
Ahrens H, Förster S, Helm C A, Naji A, Netz R R and Seidel C 2004a *J. Phys. Chem.* B **108** 16870–6
Ahrens H, Graf K and Helm C A 2001 *Langmuir* **17** 3113–5
Ahrens H, Hugenberg N, Schmidt M and Helm C A 1999 *Phys. Rev.* E **60** 4360–70
Ahrens H, Papastavrou G, Schmidt M and Helm C A 2004b *J. Phys. Chem.* B **108** 7080–91
Albrecht O, Gruler H and Sackmann E 1978 *J. Physique* **39** 301–13
Balastre M, Li F, Schorr P, Yang Y C, Mays J W and Tirrell M V 2002 *Macromolecules* **35** 9480–6

Ballauff M 2003 *Macromol. Chem. Phys.* **204** 220–34
Baltes H, Schwendler M, Helm C A and Möhwald H 1996 *J. Colloid Interface Sci.* **178** 135–43
Bates F S 1991 *Science* **251** 898–905
Beer M, Schmidt M and Muthukumar M 1997 *Macromolecules* **30** 8375–85
Dziezok P, Sheiko S S, Fischer K, Schmidt M and Möller M 1997 *Angew. Chem. Int. Edn Engl.* **36** 2812–5
Elbs H, Fukunaga K, Stadler R, Sauer G, Magerle R and Krausch G 1999 *Macromolecules* **32** 1204–11
Evans D F and Wennerström H 1994 *The Colloidal Domain: Where Physics, Chemistry, Biology, and Technology Meet* (Weinheim: VCH)
Fasolka M J and Mayes A M 2001 *Annu. Rev. Mater. Res.* **31** 323–55
Kjaer K, Als-Nielsen J, Helm C A, Laxhuber L A and Möhwald H 1987 *Phys. Rev. Lett.* **58** 2224–7
Kjaer K, Als-Nielsen J, Kenn R, Böhm C, Tippmann-Krayer P, Peterson I R, Bibo A, Helm C A, Möhwald H, Leveillier F, Jacquemain D, Weinbach S, Leiserowitz L and Deutsch M 1991 *Makromol. Chem. Macromol. Symp.* **46** 433–7
Krausch G 1995 *Mater. Sci. Eng. Rep.* **14** 1–94
Möhwald H 1993 *Rep. Prog. Phys.* **56** 653
Möhwald H, Menzel H, Helm C A and Stamm M 2004 *Adv. Polym. Sci.* **165** 151–75
Netz R R and Andelman D 2003 *Phys. Rep.* **380** 1–95
Pershan P S and Als-Nielsen J 1984 *Phys. Rev. Lett.* **52** 759
Schwartz D K, Schlossman M L, Kawamoto E H, Kellogg G J and Pershan P S 1990 *Phys. Rev.* A **41** 5687–90
Sheiko S S, Prokhorova S A, Beers K, Matyjaszewski K, Potemkin I I, Khokhlov A R and Möller M 2001 *Macromolecules* **34** 8354–60
Simister E A, Lee E M, Thomas R K and Penfold J 1992 *J. Phys. Chem.* **96** 1373
Stephan T, Muth S and Schmidt M 2002 *Macromolecules* **35** 9857–60
Wesemann A, Steitz R, Ahrens H, Förster S and Helm C A 2003 *Langmuir* **19** 709–16
Zhulina E B, Birshtein T M and Borisov O V 1995 *Macromolecules* **28** 1491